Journal of Ceramic Processing Research. Vol. 23, No. 4, pp. 430~435 (2022)
(Received 13 December 2021, Received in revised form 13 March 2022, Accepted 22 March 2022)
https://doi.org/10.36410/jcpr.2022.23.4.430

J O U R N A L O F
Ceramic Processing Research

Temperature-dependent ferroelectric and piezoelectric response of Yb^{3+} and Tm^{3+} co-doped $Ba_{0.95}Ca_{0.05}Ti_{0.90}Zr_{0.10}O_3$ lead-free ceramic

Yongshang Tian[a,*], Shuiyun Li[a], Bingqian Zhang[a], Yansheng Gong[b], Peng Liu[a], Xiongjie Hu[c] and Qiangshan Jing[a,*]

[a]*College of Chemistry and Chemical Engineering, Henan Key Laboratory of Utilization of Non-Metallic Mineral in the South of Henan, Xinyang Normal University, Xinyang 464000, China*
[b]*Faculty of Material Science and Chemistry, China University of Geosciences, Wuhan 430074, China*
[c]*Loyalty Enterprise Development (Xinyang) Co., LTd., Xinyang 464017, China*

The electrical properties of piezoelectric ceramics are temperature-dependent, which affects their potential for applications in environments with temperature variation. In this work, Yb^{3+} and Tm^{3+} co-doped $Ba_{0.95}Ca_{0.05}Ti_{0.90}Zr_{0.10}O_3$ (BCTZ-YT) dense lead-free ceramic was prepared using a modified polymeric precursor route. On the basis of structural and electrical measurements at various temperatures, the mechanism of a lack of oxygen vacancies, small structural defects, and small defect dipoles was deduced. This study reveals that the ferroelectricity and piezoelectricity are temperature-dependent, whereas the capacitance is essentially unchanged with increasing temperature owing to the presence of a pure orthorhombic phase. The capacitance of the BCTZ-YT ceramic was essentially constant at ~4.5 nF, the thermal expansion coefficient was 8.57×10^{-6} K^{-1} below 75 °C, and the piezoelectric response (d_{33}*) was above 416 pm/V in a wide temperature range (-20 to 40 °C), suggesting the results of this study are expected to inform future research.

Keywords: Yb^{3+} and Tm^{3+} co-doping, BCTZ-YT ceramics, Defects, Temperature-dependent piezoelectricity, Capacitance.

Introduction

Lead-free piezoelectric materials, i.e., materials based on $Bi_{0.5}Na_{0.5}TiO_3$, $K_{0.5}Na_{0.5}NbO_3$, $BaTiO_3$, and $BiFeO_3$, have been attracting interest because they are more environmentally friendly than lead zirconate titanate (PZT) materials [1,2]. However, lead-free piezoelectric materials are less suitable for application in electronic devices than PZT-based materials owing to their poor piezoelectric response [3]. Thus, to improve the piezoelectricity, researchers have attempted to develop lead-free materials with specific polymorphic phase transitions or a suitable morphotropic phase boundary structure similar to that of PZT-based materials [4,5]. Calcium and zirconium co-doped $BaTiO_3$ (BCTZ) is a promising candidate for use in lead-free materials; its outstanding piezoelectric constant (~700 pC/N) has attracted widespread attention for electronic device applications [6]. Doping the perovskite structure of BCTZ materials with rare earth elements or eutectic mixtures could reduce the internal stress and improve the electrical properties by reducing the number of defects [7,8].

*Corresponding author:
Tel : +86 0376 6390702
Fax: +86 0376 6390702
E-mail: tianyongshang423@163.com;
tianyongshang@xynu.edu.cn (Yongshang Tian),
9jqshan@163.com (Qiangshan Jing)

BCTZ materials co-doped with rare earth elements have electrical properties similar to those of pristine $BaTiO_3$ materials, which feature phase transformations from the hexagonal, rhombohedral, or tetragonal phase to the cubic phase with increasing temperature [9,10]. Many researchers did a lot of ingenious works on rare earth elements doped BCZT ceramics, i.e., Li et al. reported Em doped BCZT ceramics [11], Zuo et al. worked Er and Yb co-doped BCZT ceramics [12], Hamza et al. released Nd, Gd, and Y co-doped BCZT ceramics [13]. Although BCTZ materials co-doped with rare earth elements have shown excellent electrical properties, up-conversion luminescence, and thermal expansion behaviour [11-15], the temperature dependence and mechanism of the piezoelectric response and ferroelectric properties have not been extensively studied, despite its importance for practical use of these materials in electronic components. Additionally, the suitable thermophysical property, the match of expansion behaviour of the substrate and matrix ceramic materials, was one of decisive factors for their long service life in actual application [16-18].

In this work, the temperature-dependent electrical properties of Yb^{3+} and Tm^{3+} co-doped $Ba_{0.95}Ca_{0.05}Ti_{0.90}Zr_{0.10}O_3$ lead-free ceramics were prepared using a modified polymeric precursor method. The capacitance, thermal expansion behaviour, and fracture strength were also reported. Effects of these defects, vacancies, and defect dipoles on the temperature dependence of the ferro-

electricity, piezoelectricity, and permittivity were systematically studied. Additionally, thermophysical property of the ceramic was also researched. The results provide valuable insights into their application in environments with temperature variation.

Experimental Procedure

Materials preparation

Stoichiometric $Ba_{0.95-x}Ca_{0.05}Ti_{0.90}Zr_{0.10}O_3$-0.7mol%Yb-0.5mol%Tm (abbreviated as BCTZ-YT; x = 0.012) lead-free ceramic nanoparticles were prepared using a modified polymeric precursor method reported in our previous work [19], using $Ba(CH_3COO)_2$, $Ca(NO_3)_2 \cdot 4H_2O$, $Ti(OC_4H_9)_4$, $Zr(NO_3)_4 \cdot 5H_2O$, $Yb(NO_3)_3 \cdot 5H_2O$, $Tm(NO_3)_3 \cdot 6H_2O$, citric acid, and ethylene glycol monomethyl ether as the raw materials. The nanoparticles were mixed with 2.5 wt.% polyvinyl alcohol and pressed by cold isostatic pressing at 200 MPa to obtain a disc-shaped green body with 10 mm in diameter and ~0.8 mm in thickness. After burning out the polyvinyl alcohol binder at 650 °C for 2 h at porcelain boat, the green body was sintered in air at 1240 °C for 5 h to obtain the BCTZ-YT ceramic. Silver electrodes were coated on both polished parallel discs sides of the ceramic to examine the electrical properties. Then, the sample was polarized in silicone oil bath at 25 °C for 30 min by applying a direct-current electric field of 15 kV/cm, the subsequent piezoelectric response was characterized after 36 h in air dry oven.

Characterization

The phases of the sample were identified by X-ray diffraction (XRD; X'Pert-Pro, Holland) using Cu Kα radiation at a 2θ scanning rate of 0.05°/s. Scanning electron microscopy (SEM; S4800) coupled with energy dispersive spectrometry (EDS) was used to measure the fresh fracture surface. The electron binding energy the BCTZ-YT ceramic was investigated using X-ray photoelectron spectroscopy (XPS, K-ALPHA, UK). The permittivity was measured using a dielectric measurement system (HDMS-1000V, Partulab, P.R. China). A Radiant precision workstation (RTI-Multiferroic II, USA) was used to detect the polarisation-electric field (*P*-*E*) hysteresis loops, leakage current, capacitance, and resistivity. The strain-electric field (*S*-*E*) loops were measured by an optical reflectance sensor (MTI-2100, USA). To measure the fracture strength and thermophysical performance, the BCTZ-YT ceramic was cut into ~12 mm × ~5 mm × ~1 mm samples after the silver electrodes were removed from the surface using grinding paper. The fracture strength of the ceramic was estimated using a motorised bending tester (KZJ-300N, P.R. China). A precision electronic balance (ED-124S) was used to detect the densification of the BCTZ-YT ceramic according to the Archimedes principle. The coefficient of thermal expansion (*CTE*) was examined using a dilatometer (DIL 402, Netzsch, Germany).

Results and Discussion

Fig. 1 shows the XRD pattern of the BCTZ-YT ceramic and the Rietveld-refined XRD pattern for the *Amm*2 space group obtained using the Fullprof software. The sample was found to have a pure orthorhombic phase (JCPDS Card No. 81-2200) with perovskite (ABO_3) structure and no secondary phase, indicating that the ytterbium and thulium entered the ABO_3 crystal lattice successfully [20]. Moreover, the single orthorhombic phase of the BCTZ-YT ceramic at room temperature could be also explored by the subsequent temperature dependence of the relative permittivity results in this study. The fitting parameters, R_p = 0.037, R_{wp} = 0.060, and χ^2 = 0.31, indicated that the fitting procedure was highly accurate. The fitted lattice parameters were a = 3.906 Å, b = 5.559 Å, and c = 5.577 Å, and the axial angle was 90°.

Fig. 2 shows a scanning electron microscopy image of the fracture surface and the elemental distributions. It could be detected the BCTZ-YT ceramic underwent high densification (relative density, 96.37%; Table 1) and has a high fracture strength (71.43 MPa), with an average grain size of ~0.92 μm. The elemental distributions in the BCTZ-YT ceramic suggest that Ba, Ca, Yb, Tm, Ti, Zr, and O are uniformly distributed in the structure. The homogeneous dispersion of the elements could hold back the local element disturbance effect and stabilize electrical performance.

Fig. 3 shows the temperature dependence of the relative permittivity (ε_r) and loss tangent (tan δ) of the BCTZ-YT ceramic at 100 Hz, 1 kHz, 10 kHz, and 100 kHz. The permittivity peak at ~115 °C indicates the cubic-to-tetragonal phase transition temperature (T_C; Curie temperature), and the permittivity peak at ~45 °C

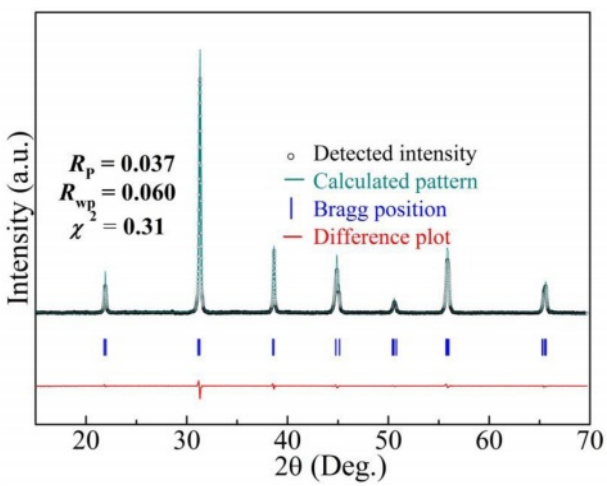

Fig. 1. Detected and Rietveld-refined XRD patterns of the BCTZ-YT ceramic obtained using Fullprof software.

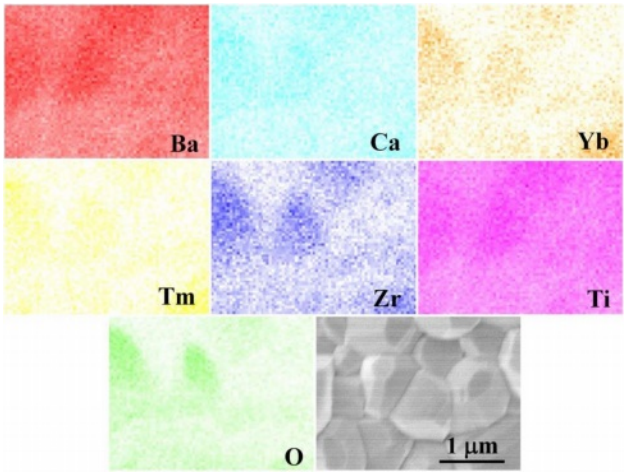

Fig. 2. EDS results showing the Ba, Ca, Yb, Tm, Ti, Zr, and O distributions, and SEM image of the fracture morphology of the BCTZ-YT ceramic.

Table 1. Density, relative density (ρ_r), and fracture strength (K) of the BCTZ-YT ceramic.

Category	Density (g/cm^3)	ρ_r (%)	K (MPa)
BCTZ-YT ceramic	5.702	96.37	71.43

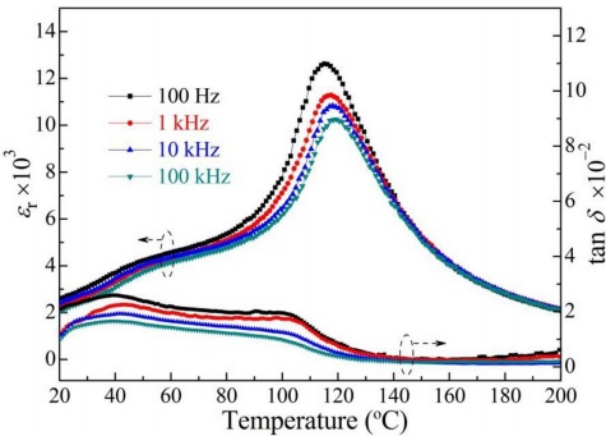

Fig. 3. Temperature dependence of the relative permittivity (ε_r) and loss tangent (tan δ) of the BCTZ-YT ceramic at various frequencies.

indicates the orthorhombic-to-tetragonal phase transition temperature ($T_{O\text{-}T}$). The BCTZ-YT ceramic showed low tan δ values (~0.02) at various frequencies, which could be attributed to the high densification of the ceramic with small flaws in its structure. The ε_r values decreased with increasing frequency because of the slight interfacial polarisation and reduced charge accumulation at the grain boundaries [21]. The light frequency dispersion of the permittivity indicates that the ceramic may have typical ferroelectricity [22]. Moreover, the low loss tangents implied that the ceramic might possess high density, with small flaws and few oxygen vacancies.

Fig. 4 displays the electron binding energy of the

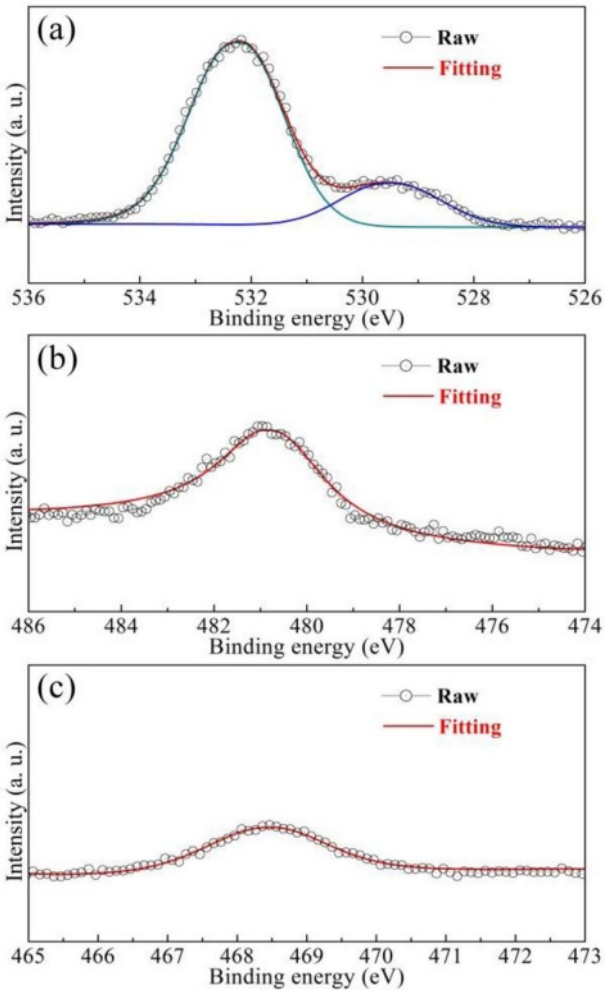

Fig. 4. (a) O 1s, (b) Yb 4s, and (c) Tm 4s XPS spectra of the BCTZ-YT ceramic at 20 °C.

BCTZ-YT ceramic. The peak at 532.2 eV (Fig. 4(a)) represents the cation-oxygen bonds (O 1s), whereas the peak at 529.6 eV corresponds to oxygen vacancies as well as absorbed H_2O on the surface. The peaks at 480.9 eV (Fig. 4(b)) and 468.5 eV (Fig. 4(c)) represent Yb 4s (the +3 state) and Tm 4s (the +3 state), respectively [23,24]. The results suggested that Yb^{3+} and Tm^{3+} ions could exist stably in the ceramic, and the volume of oxygen vacancies was just a little in the structure. The mechanism of the small defect dipoles as lack of oxygen vacancies of the BCTZ-YT ceramic is given by Eq. (1) [25].

$$Yb^{3+} + Tm^{3+} + V_O^{\cdot\cdot} + \frac{1}{2}O_2(g) \xrightarrow{BCZT} Yb'_{Ba/Ca} + Tm'_{Ba/Ca} + O_O^{\times} \quad (1)$$

Fig. 5 shows the temperature dependence of the inverse permittivity ($10^4/\varepsilon_r$) of the BCTZ-YT ceramic at a frequency of 10 kHz at various temperatures. The definitions of each parameter are also shown in the Fig. 5, where T_{CW} is the Curie-Weiss temperature, T_m is the temperature of maximum permittivity, T_B is the

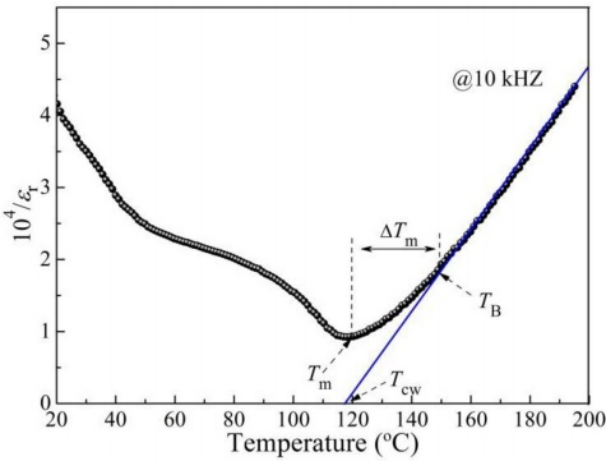

Fig. 5. Inverse permittivity ($10^4/\varepsilon_r$) of the BCTZ-YT ceramic at a frequency of 10 kHz at various temperatures.

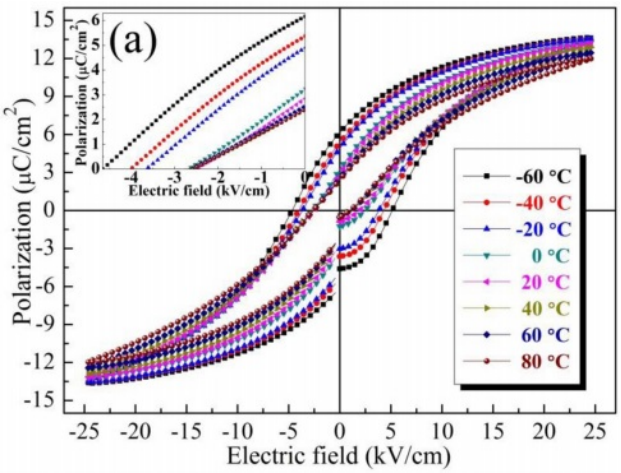

Fig. 6. Polarisation-electric field (*P-E*) hysteresis loops of the BCTZ-YT ceramic. The inset (a) show an enlarged view of a selected region (−4.9 to 0 °C) of the *P-E* loops.

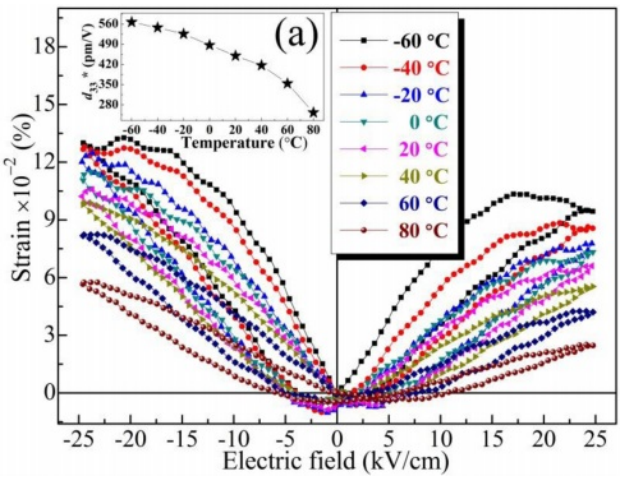

Fig. 7. Strain-electric field (*S-E*) loops and piezoelectric coefficient (d_{33}*, inset (a)) of the BCTZ-YT ceramic at various temperatures.

temperature at which the permittivity begins to follow the Curie-Weiss law, and ΔT_m is the temperature deviation, which indicates the level of dielectric diffusion. These fitted parameters were introduced to investigate the quantitative parameters of the diffuse phase transition using the Curie-Weiss law (Eqs. (2) and (3)). T_m, T_{CW}, T_B, and ΔT_m were found to be 120.40, 117.40, 149.54, and 29.14 °C, respectively.

$$\frac{1}{\varepsilon_r} = \frac{T - T_C}{C} \tag{2}$$

$$\Delta T_m = T_B - T_m \tag{3}$$

where C is the Curie-Weiss parameter, which also indicates the degree of the diffuse phase transition. The weak diffuse phase transition (ΔT_m, 29.14 °C) was also demonstrated the BCTZ-YT ceramic possesses good ferroelectricity. This finding could be attributed to the presence of fewer imbalanced local charges at the grain boundaries and the small crystal flaws in the structure [26].

To further investigate the ferroelectricity and piezoelectricity of the ceramic, the polarisation-electric field (*P-E*) hysteresis loops (Fig. 6) and the strain-electric field (*S-E*) loops and piezoelectric coefficient at various temperatures (Fig. 7) were obtained. As shown in Fig. 6, the remanent polarisation (P_r) of the ceramic decreased from 6.1 to 2.4 μC/cm^{-2} with increasing temperature (<80 °C), and the coercive field (E_c) also decreased. The decrease in ferroelectricity (that is, the absence of typical saturated hysteresis) at high temperature was associated with the increased structural symmetry. With the increment of testing temperature, the ceramic orthorhombic symmetry transformed to tetragonal symmetry around 60 °C, accompanying the deteriorated P_r, which was associated with the polarisation rotation of dipoles became harder as phase evolution [27,28]. Moreover, the continued appearance of the *P-E* loops at high temperature (higher than the Curie temperature, T_C) resulted from the formation of polar nanoregions in the structure [27]. The decrease in the coercive field at high temperature was attributed to easy dipole switching. Moreover, the low E_c value was attributed to the low internal stress resulting from small defects in the structure, which was consistent with the results in Fig. 4. As shown in Fig. 7, the piezoelectric response (d_{33}*) clearly decreased (from 562 to 241 pm/V) with increasing temperature, which was due to the transformation from ferroelectric to paraelectric phase in the BCTZ-YT ceramic with increment of the temperature [28].

To further investigate the structural defects in the BCTZ-YT ceramic at 20 °C, the thermal expansion behaviour were also measured. Fig. 8 shows the coefficients of thermal expansion (*CTE*) of the BCTZ-YT ceramic, which affect its service life. Two curves were

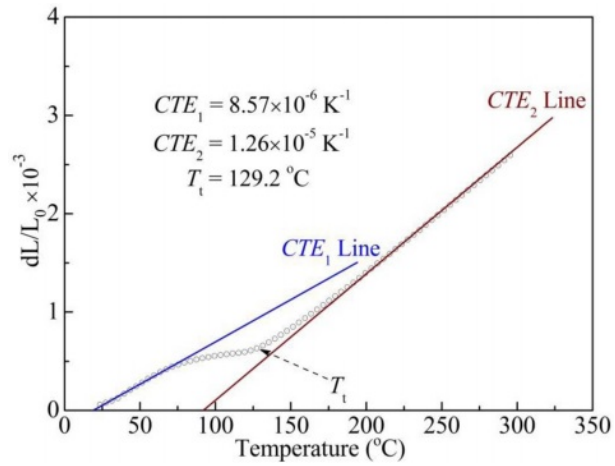

Fig. 8. Coefficients of thermal expansion (*CTE*) of the BCTZ-YT ceramic at various temperatures.

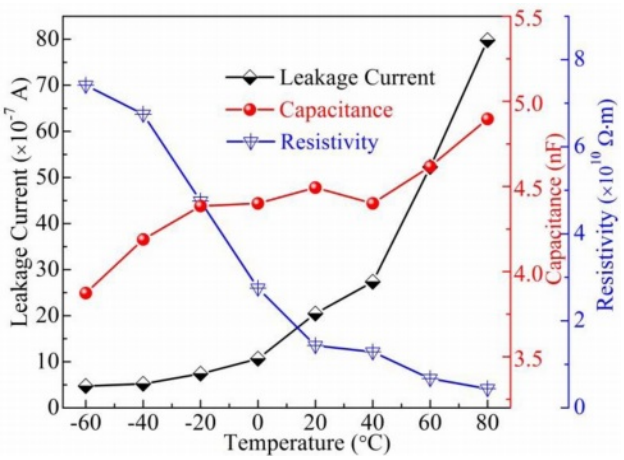

Fig. 9. Leakage current, capacitance, and resistivity of the BCTZ-YT ceramic at various temperatures.

fitted, at temperatures below 75 °C (CTE_1) and above 180 °C (CTE_2), suggesting that the lattice expansion behaviour of the ceramic varied with temperature. CTE_1 (8.57×10^{-6} K^{-1}) was smaller than CTE_2 (1.26×10^{-5} K^{-1}), implying the thermal expansion of the orthorhombic ferroelectric phase was weaker than that of the cubic paraelectric phase of the BCTZ-YT ceramic, because of the needed energy of switched domain dipoles in orthorhombic phase was higher than that of the cubic phase. Moreover, the low level *CTE* value suggested that the BCTZ-YT ceramic might have small structural defects, which was consistent with the presence of weak structural defects [29].

Fig. 9 shows the leakage current, capacitance, and resistivity of the BCTZ-YT ceramic at various temperatures. The leakage current increased gradually with increasing temperature; this behaviour was attributed to faster charge transfer resulting from the easy dipole switching [30]. The faster charge transfer also caused the resistivity of the BCTZ-YT ceramic to decrease with increasing temperature. The capacitance of the BCTZ-YT ceramic was essentially constant at ~4.5 nF in a wide temperature range (-20 to 40 °C), whereas the other electrical properties temperature-dependent. Firstly, the constant capacitance could be attributed to the fact that only the orthorhombic phase was present in the tested temperature range, as shown in Fig. 1. Secondly, the constant capacitance might be associated with the stable value of grain capacitance under the temperature range [31]. Moreover, the result shows that the capacitance elevated owing to the phase transformation (Fig. 3) with further increasing temperature.

Conclusions

A BCTZ-YT ceramic was prepared, and the temperature dependence of its electrical properties was investigated. A series of structural and electrical measurements demonstrated that the ceramic had small structural defects, few oxygen vacancies, and small defect dipoles. A formula explaining the lack of oxygen vacancies was presented. The ferroelectricity and piezoelectricity of the ceramic decreased with increasing temperature because the dipoles switched more easily at higher temperature. The leakage current of the ceramic increased with increasing temperature, whereas the resistivity showed the opposite tendency. The capacitance was essentially constant because only a single orthorhombic phase was present, although at higher temperatures it increased with increasing temperature after a phase transformation. In addition, thermal expansion coefficient (*CTE*) was also displayed for stating their thermophysical performance. This work is expected to provide useful ideas for further research on the characteristics of BCTZ lead-free ceramics at various temperatures.

Acknowledgements

This work was supported by the Youth Talent Support Project of Henan Province of China (2021HYTP019), the Key Youth Scholar Funding Project of Henan Province of China (2021GGJS097), and Henan Province Science and Technology Research Project (222102230024). The authors would like to thank the Analysis & Testing Center of XYNU for their testing help.

References

1. H. Tao, H. Wu, Y. Liu, Y. Zhang, J. Wu, F. Li, X. Lyu, C. Zhao, D. Xiao, J. Zhu, and S. Pennycook, J. Am. Chem. Soc. 141[35] (2019) 13987-13994.
2. J. Rödel, K. Webber, R. Dittmer, W. Jo, M. Kimura, and D. Damjanovic, J. Eur. Ceram. Soc. 35 (2015) 1659-1681.
3. E. Cross, Nature 432 (2004) 24-25.
4. W. Li, Z. Xu, R. Chu, P. Fu, and G. Zang, Physica B 405[21] (2010) 4513-4516.
5. A. Ghandouri, S. Sayouri, T. Lamcharfi, and L. Hajjic, J. Ceram. Process. Res. 19[2] (2018) 154-170.

6. W. Liu, and X. Ren, Phys. Rev. Lett. 103 (2009) 257602.
7. T. Zheng, J. Wu, D. Xiao, and J. Zhu, Prog. Mater. Sci. 98 (2018) 552-624.
8. W. Yang, B. Zhang, N. Ma, and L. Zhao, J. Eur. Ceram. Soc. 32 (2012) 899-904.
9. Y. Feng, J. Wu, Q. Chi, W. Li, Y. Yu, and W. Fei, Chem. Rev. 120 (2020) 1710-1787.
10. J. Hao, W. Li, J. Zhai, and H. Chen, Mat. Sci. Eng. R. 135 (2019) 1-57.
11. Q. Li, Q. Zhang, W. Cai, C. Zhou, R. Gao, G. Chen, X. Deng, Z. Wang, and C. Fu, Mater. Chem. Phys. 252 (2020) 123242.
12. Q. Zuo, L. Luo, and Y. Yao, J. Alloy. Compd. 632 (2015) 711-716.
13. A. Hamza, F. Benabdallah, I. Kallel, L. Seveyrat, L. Lebrun, and H. Khemakhem, J. Alloy. Compd. 735 (2018) 2523-2531.
14. J. Shi, X. Lu, J. Shao, B. Fang, S. Zhang, Q. Du, J. Ding, X. Zhao, and H. Luo, Ferroelectrics 507 (2017) 186-197.
15. Y. Tian, L. Cao, Y. Zhang, Y. Jing, X. Ji, Y. Gong, S. Sun, and Q. Jing, Ceram. Int. 46 (2020) 10040-10047.
16. R. Hayati, M. Fayazi, H. Diargar, M. Kaveh, and L. Tayebi, Int. J. Appl. Ceram. Tec. 17[4] (2020) 1891-1898.
17. G. Messing, S. Poterala, Y. Chang, T. Frueh, E. Kupp, B. Watson, R. Walton, M. Brova, A. Hofer, R. Bermejo, and R. Meyer, J. Mater. Res. 32 (2017) 3219-3241.
18. Y. Yang, S. Jeong, J. Kwak, and S. Lee, J. Ceram. Process. Res. 17[7] (2016) 747-751.
19. Y. Tian, S. Li, Y. Gong, D. Meng, J. Wang, and Q. Jing, J. Alloy. Compd. 692 (2017) 797-804.
20. L. Zeng, R. Benioub, and K. Itaka, J. Ceram. Process. Res. 23[1] (2022) 62-68.
21. M. Hu, S. Li, and C. Wang, Appl. Surf. Sci. 509 (2020) 145314.
22. Q. Wei, M. Zhu, M. Zheng, and Y. Hou, Mater. Chem. Phys. 249 (2020) 122966.
23. J. Lv, X. Lou, and J. Wu, J. Mater. Chem. C 4[25] (2016) 6140-6151.
24. Z. Li, J. Wu, D. Xiao, J. Zhu, and W. Wu, Acta Mater. 103 (2016) 243-251.
25. J. Wu, Z. Wu, W. Mao, and Y. Jia, Mater. Lett. 149 (2015) 74-76.
26. I. Coondoo, N. Panwar, H. Amorín, M. Alguero, and A. Kholkin, J. Appl. Phys. 113 (2013) 214107.
27. J. Wu, A. Mahajan, L. Riekehr, H. Zhang, B. Yang, N. Meng, Z. Zhang, and H. Yan, Nano Energy 50 (2018) 723-732.
28. Q. Xu, D. Zhan, H. Liu, W. Chen, D. Huang, and F. Zhang, Acta Mater. 61[12] (2013) 4481-4489.
29. Q. Xu, D. Huang, W. Chen, F. Zhang, and B. Wang, J. Alloy. Compd. 429 (2007) 34-39.
30. T. Badapanda, S. Sarangi, B. Behera, S. Parida, S. Saha, T. Sinha, R. Ranjan, and P. Sahoo, J. Alloy. Compd. 645 (2015) 586-596.
31. I. Coondoo, N. Panwar, R. Vidyasagar, and A. Kholkin, Phys. Chem. Chem. Phys. 18 (2016) 31184-31201.